



# Experimental investigation and numerical modeling of oxidative pyrolysis mechanism of mining PVC cable sheath

Jinlong Zhao<sup>1,2</sup> · Hanchao Ma<sup>2,3</sup> · Hong Huang<sup>3</sup> · Jianping Zhang<sup>4</sup> · Youliang Chen<sup>5</sup>

Received: 26 January 2022 / Accepted: 16 October 2022 / Published online: 4 November 2022  
© The Author(s) 2022

## Abstract

Cables modified with flame retardants are widely used in the coal mining process to enhance their fire safety performance. This paper investigates experimentally and numerically the thermo-oxidative degradation process of PVC-based mining cable sheath, which consists of PVC resin and plasticizers (Phthalate esters), fillers (Calcium carbonate), and flame retardant (Antimony trioxide) as additives. Thermogravimetry coupled with Fourier transform infrared spectroscopy (TG-FTIR) experiments were performed at different heating rates in an air atmosphere. TG results showed that the decomposition processes of mining PVC cable sheath are more complicated than those of pure PVC with additional degradation steps, which was further confirmed by FTIR gas analysis. A deconvolution method was used to distinguish the independent reactions from the overlapped derivative thermogravimetric (DTG) peaks. It was found that the whole degradation process can be divided into seven steps, based on which an oxidative pyrolysis model was developed: pyrolysis of plasticizers (steps 1 and 2), dehydrogenation (step 3), emission and combustion of volatile fraction (step 4), carbon combustion (step 5), oxidative pyrolysis of complicated additives (step 6), and decomposition of residues (step 7). The kinetic triplets (activation energy, pre-exponential factor, and reaction model function) for each reaction were firstly calculated using three commonly used model-free methods and then further optimized using the genetic algorithm (GA). Based on the optimized parameters, the reaction mechanisms and their associated kinetic parameters were determined. The findings of this study are important in understanding the oxidative pyrolysis process of PVC cable sheath, and the obtained kinetic parameters can also be used for its pyrolysis and fire modeling, waste recycling, and risk assessment.

**Keywords** PVC cable sheath · Oxidative pyrolysis · Reaction kinetics · Deconvolution, generative algorithm · TG-FTIR

## Introduction

Cables play a significant role in the safety production process of coal mines. In recent years, attention has been increasingly paid to the fire safety in the mining industry following

major incidents involving cable fires. Due to their highly flammable nature, cables with increased fire retardancy are required to be used in underground coal mines. Although the main components of cable materials (e.g., PVC material for communication cable sheath layers) are specified in the current standard, the additives and flame retardants have however not been clearly stated. In a real underground cable fire, despite the fact that the flame retardants can prevent cable fire to some extent, the addition of complex additives may lead to uncertain thermal response and release toxic gases [1–3], causing severe economic losses to society and harm to human health. For instance, on January 5th, 2010, a cable fire accident occurred in Lisheng Coal Mine. The short circuit of cables ignited the cable sheath and surrounding coal seam, resulting in 34 deaths and a direct economic loss of 29.62 million RMB [4]. Hence, to prevent mining cable fire, it is necessary to conduct a risk assessment for cable fires and develop new fire standards for mining cable

✉ Jianping Zhang  
j.zhang@ulster.ac.uk

<sup>1</sup> State Key Laboratory of Coal Resources and Safe Mining, China University of Mining & Technology, Beijing, China

<sup>2</sup> School of Emergency Management & Safety Engineering, China University of Mining & Technology, Beijing, China

<sup>3</sup> Institute of Public Safety Research, Department of Engineering Physics, Tsinghua University, Beijing, China

<sup>4</sup> FireSERT, Belfast School of Architecture and the Built Environment, Ulster University, Newtownabbey, UK

<sup>5</sup> China Academy of Safety Science & Technology, Beijing, China

materials, and these works are closely related to the thermal degradation characteristics of cable materials.

Extensive studies have been conducted to examine the pyrolysis characteristics of commercial cables [5–8]. However, few studies investigated the oxidative pyrolysis process of mining cable sheath with an emphasis on the effects of the additives. The understanding of the influence of additives on the thermal oxidative degradation process of PVC cables can assist us in resolving fire modeling, waste recycling, and risk assessment problems. By examining the fire behavior of flame-retarded cables in relation to the oxidative pyrolysis steps of PVC materials, the degradation process of mining cables in the air atmosphere can also be used to explain the flame propagation process in large-scale experiments [9].

Thermogravimetry (TG) coupled with Fourier transform infrared spectroscopy (FTIR) is often used to analyze the oxidative pyrolysis and gas release process of PVC materials. Wang et al. [10] investigated the thermal behavior of PVC by TG-FTIR and divided the oxidative pyrolysis process into three main stages: dehydrogenation, combustion of the volatile matter, and carbon combustion. Zhou et al. [11] studied the composition of volatiles during the pyrolysis of PVC by TG-FTIR and pyrolysis–gas chromatography/mass spectrometry (Py-GC/MS). They found that the volatiles are mainly composed of hydrochloric acid (HCl), chlorinated hydrocarbons, alkenes, and aromatics. Aracil et al. [12] proposed an oxidative pyrolysis model based on a multi-step model-fitting method of TG data to describe the degradation process of pure PVC. Bhargava et al. [13] used an isoconversional method and a distributed reactivity model to study the thermal decomposition kinetics of PVC, and the simulation result showed a good agreement with the experimental data.

The degradation behavior of PVC cable sheath has also been studied by several researchers [5, 6, 14, 15]. Beneš et al. [5] investigated the thermal degradation process of commercial PVC cables by TG-FTIR and found that the plasticizer started to pyrolyze in the temperature range of 200–340 °C, in which di-n-octyl phthalate gas was detected. In addition, they found that the last degradation process can be contributed to the CaCO<sub>3</sub> decomposition. Brebu et al. [6] studied the characterization of high-voltage electrical cable insulation waste by TG and reported a shoulder peak in the pyrolysis rate at around 310 °C which was attributed to the presence of the plasticizer in the cables. Wang et al. [14] investigated the thermal behavior of flame-retarded high-voltage cable sheath and observed that the second pyrolysis peak can be partly attributed to the structural rearrangement between PVC and additives. Wang et al. [15] carried out a thermal kinetics study on new and aged commercial cables and reported noticeable difference between the experimental and predictive values, due to the additives in the cables.

Existing studies have clearly demonstrated that there is a significant difference in the oxidative pyrolysis process

between PVC cables and pure PVC due to the presence of the additives. While the effects of additives on the oxidative pyrolysis process have been reported, detailed and comprehensive modeling of the oxidative pyrolysis mechanism of mining cables is still limited. In this study, mining PVC cable sheath consisting of a PVC resin, plasticizers (Phthalate esters), fillers (Calcium carbonate) and flame retardant (Antimony trioxide) was selected to investigate the degradation process with an emphasis on the effects of the additives. The thermal behavior and the corresponding gas release process of the cable sheath were firstly analyzed by TG-FTIR, based on which a deconvolution procedure was used to identify the individual reactions and their associated peaks. Subsequently, the kinetic parameters of each of the reactions were calculated by three model-free methods coupled with a generalized master-plot method. Finally, the kinetic parameters were further optimized using the genetic algorithm (GA) in comparison with the experimental measurements.

## Experimental method and kinetic analysis

### Experimental method

The mining PVC cable sheath used in this study was composed of PVC resin, plasticizers (Phthalate esters), fillers (Calcium carbonate) and flame retardant (Antimony trioxide, Sb<sub>2</sub>O<sub>3</sub>, 4% by mass), supplied by Hebei Xiangtai Cable Co., Ltd. The cable product has been certified by the coal industrial standard (MT818.14–1999). Samples were pre-cut into approximately uniform pieces and tested in an STA449-F3 Synchronous Thermal Analyzer (Netzsch Company) coupled with a Tensor27 Fourier Transform Infrared Spectrometer (Bruker Company). For each experiment, the sample mass was 10 ± 0.1 mg. The samples were heated from 303 to 1273 K at constant heating rates. The gas flow rate was 100 mL min<sup>-1</sup>. The infrared spectrum of the pyrolysis gases was analyzed using the FTIR connected to the thermal analyzer through a tube. The temperature of the tube and the FTIR gas chamber was kept at 473 K to prevent condensation. The infrared spectrum scanning wave number range was 400 ~ 4000 cm<sup>-1</sup>.

Tests were conducted in the air atmosphere at four heating rates: 2, 5, 10, and 15 K min<sup>-1</sup>. At least two runs were performed for each heating rate to ensure the repeatability of the tests. To investigate the influence of the atmosphere and initial sample mass on the pyrolysis process, two additional tests were carried out in nitrogen (10 mg) and in air (5 mg) at a heating rate of 10 K min<sup>-1</sup>. The data, not included here for brevity, confirmed that the initial sample mass has no influence on the results.

### Kinetic analysis

For single-step degradation of a solid, the decomposition rate can be described as follows [16]:

$$\frac{d\alpha}{dt} = A \exp\left(-\frac{E_a}{RT}\right) f(\alpha) \tag{1}$$

where  $t$  is the time, s;  $T$  is the sample temperature, K;  $A$ ,  $E_a$  and  $f(\alpha)$  denote, respectively, the pre-exponential factor,  $s^{-1}$ , activation energy,  $kJ\ mol^{-1}$ , and reaction model function;  $R$  is the universal gas constant,  $8.314\ J\ mol^{-1}\ K^{-1}$ ; and  $\alpha$  refers to the degree of conversion defined as

$$\alpha = \frac{m_0 - m_t}{m_0 - m_\infty} \tag{2}$$

where  $m_0$ ,  $m_t$ , and  $m_\infty$  are the initial mass, the remaining mass at a time  $t$ , and the final residual mass of the sample, respectively.

When the temperature increases linearly with time, the heating rate  $\beta$  can be expressed as

$$\beta = \frac{dT}{dt} = \text{constant} \tag{3}$$

Substituting Eq. (3) into Eq. (1), one obtains

$$\frac{d\alpha}{dT} = \frac{A}{\beta} \exp\left(-\frac{E_a}{RT}\right) f(\alpha) \tag{4}$$

The kinetic triplets ( $A$ ,  $E$  and  $f(\alpha)$ ) are needed for describing each of the reactions and their determination based on kinetic analysis will be discussed next.

### Deconvolution procedure

Reactions of PVC cable sheath are complex and involve several overlapping processes and, as a result, the kinetic analysis of their reactions and the determination of the kinetic parameters are challenging. To divide the overlapped peaks into individual ones, mathematical deconvolution analysis was recommended and widely used by ICTAC [17–19]. This method uses a mathematical function  $F(T)$  to estimate independent reaction peaks from the overlapped ones:

$$\frac{d\alpha}{dT} = \sum_{i=1}^N F(T) \tag{5}$$

where  $N$  is the number of pre-set reaction steps in the whole degradation process.

Among different mathematical functions, the Weibull distribution function has been shown to nicely fit the kinetic curves of complex solid reactions as demonstrated

for wheat straw oxidative pyrolysis [18] and animal bones combustion [19], and as a result is used in this study.

$$F(T) = a_0 \left(\frac{a_3 - 1}{a_3}\right)^{\frac{1-a_3}{a_3}} \left(\frac{T - a_1}{a_2} + \left(\frac{a_3 - 1}{a_3}\right)^{\frac{1}{a_3}}\right)^{a_3 - 1} \exp\left[-\left(\frac{T - a_1}{a_2} + \left(\frac{a_3 - 1}{a_3}\right)^{\frac{1}{a_3}}\right)^{a_3} + \frac{a_3 - 1}{a_3}\right] \tag{6}$$

where  $a_0$ ,  $a_1$ ,  $a_2$  and  $a_3$  are, respectively, the amplitude, center, width and shape of each reaction.

Based on Eqs. (5) and (6), by pre-setting the number of reaction steps  $N$ , the contribution of each reaction step on the degradation process can be estimated in the form of  $F(T)$ , and by cumulating the  $F(T)$  values of all reactions, a non-linear curve fitting for the experimental data can be used to estimate the parameters of  $F(T)$  which represent possible parallel reactions [20]. The obtained individual peaks that correspond to independent reactions will provide a basis for the calculation of the kinetic triplets.

### Calculation of kinetic triplets

Three model-free methods, namely Flynn–Wall–Ozawa (FWO) method [21–23] Kissinger–Akahira–Sunose (KAS) method [24] and Friedman (FR) method [25], were widely used to calculate the activation energy of each reaction, as shown below:

$$\ln\beta = \ln\left(\frac{AE_a}{Rg(\alpha)}\right) - 5.331 - 1.052\left(\frac{E_a}{RT}\right) \tag{7}$$

$$\ln\frac{\beta}{T^2} = \ln\left(\frac{AE_a}{Rg(\alpha)}\right) - \frac{E_a}{RT} \tag{8}$$

$$\ln\left(\beta \frac{d\alpha}{dT}\right) = \ln(f(\alpha)A) - \frac{E_a}{RT} \tag{9}$$

where  $g(\alpha)$  denotes the integral form of the reaction model function.

By drawing the  $\ln\beta-1/T$  plots (FWO method),  $\ln\beta/T^2-1/T$  plots (KAS method) and  $\ln(\beta \frac{d\alpha}{dT})-1/T$  plots (FR method) at different degrees of conversion, the corresponding activation energy  $E_a$  can be obtained from the slope of the plots as a function of  $\alpha$ .

To determine the reaction mechanism function  $f(\alpha)$ , the generalized master-plots method [26] was employed:

$$\frac{f(\alpha)}{f(0.5)} = \frac{(\frac{d\alpha}{dT})_\alpha \exp(E/RT_\alpha)}{(\frac{d\alpha}{dT})_{0.5} \exp(E/RT_{0.5})} \tag{10}$$

where  $f(\alpha)$ ,  $f(0.5)$ ,  $(\frac{d\alpha}{dt})_\alpha$ ,  $(\frac{d\alpha}{dt})_{0.5}$ ,  $T_\alpha$ , and  $T_{0.5}$  represent the reaction model value, reaction rate value and

corresponding temperatures when the conversion degree equals to  $\alpha$  and 0.5, respectively.

If we calculate, for different values of  $\alpha$ ,  $\frac{(d\alpha/dT)_\alpha \exp(E/RT_\alpha)}{(d\alpha/dT)_{0.5} \exp(E/RT_{0.5})}$  from the TG experimental data and then

plot  $\frac{f(\alpha)}{f(0.5)}$  against  $\alpha$ , the appropriate reaction mechanism  $f(\alpha)$  for each reaction can be determined based on best fitting. Some of the common reaction models are included in the Supplementary Materials (Table S1) [16], among which the Truncated Sestak-Berggren (SB) model, an empirical relation, can be used to fit any reaction. After the estimation of  $E$  and  $f(\alpha)$ , the pre-exponential factor  $A$  can be calculated by the Friedman (FR) method using Eq. (9).

### Result optimization

As a widely used nonlinear regression fitting method in optimization of kinetic triplets, the genetic algorithm (GA) can perform a global search considering mutation and crossover [7]. By taking the values of  $E$ ,  $\ln A$  and  $f(\alpha)$  found from the model-free methods and generalized master-plot method as the initial estimates, the final kinetic parameters can be obtained through the GA optimization.

The objective function (OF) of a GA search focuses on minimizing the errors between experimental and calculated values:

$$\text{OF} = \sum_{i=1}^N \frac{\sum_{j=1}^M \left( \left( \frac{d\alpha}{dT} \right)_{ij}^{\text{exp}} - \left( \frac{d\alpha}{dT} \right)_{ij}^{\text{cal}} \right)^2}{\sum_{j=1}^M \left( \left( \frac{d\alpha}{dT} \right)_{ij}^{\text{exp}} - \left( \frac{d\alpha}{dT} \right)_i^{\text{exp}} \right)^2} \quad (11)$$

where  $N$  denotes the number of tests at different heating rates,  $M$  is the number of data points for each test.  $\left( \frac{d\alpha}{dT} \right)_{ij}^{\text{exp}}$  is the measured value from the experiments,  $\left( \frac{d\alpha}{dT} \right)_{ij}^{\text{cal}}$  is the calculated value based on Eq. (4) and  $\left( \frac{d\alpha}{dT} \right)_i^{\text{exp}}$  is the average value of  $\left( \frac{d\alpha}{dT} \right)_{ij}^{\text{exp}}$ .

Using the objective function, the fitting error  $\varphi$  for each test can be calculated as

$$\varphi = \frac{\sum_{j=1}^M \left( \left( \frac{d\alpha}{dT} \right)_j^{\text{exp}} - \left( \frac{d\alpha}{dT} \right)_j^{\text{cal}} \right)^2}{\sum_{j=1}^M \left( \left( \frac{d\alpha}{dT} \right)_j^{\text{exp}} - \left( \frac{d\alpha}{dT} \right)^{\text{exp}} \right)^2} \quad (12)$$

## Results and discussion

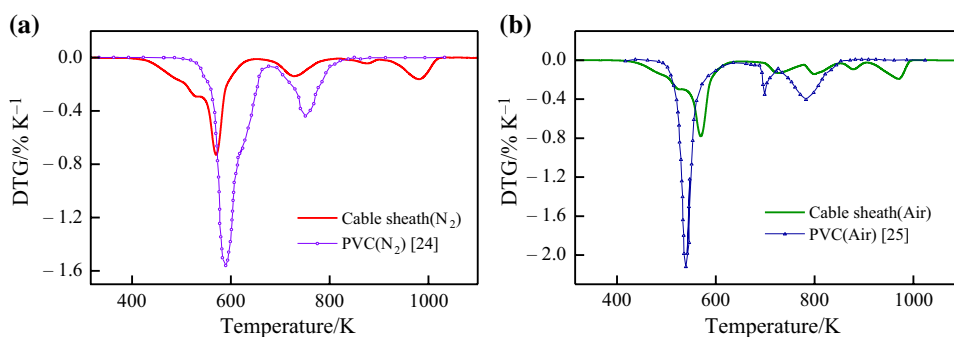
### Thermogravimetric analysis

Figures 1a and 1b show the comparisons of the decomposition rate (DTG) of PVC cable sheath and pure PVC under air and nitrogen atmospheres.

Compared with pure PVC [7, 27], the pyrolysis process of PVC cable sheath is more complex. The onset thermal degradation temperature (420 K) of PVC cable sheath is lower than that of pure PVC (500 K) due to the decomposition of the plasticizers at lower temperatures. The decrease in the DTG<sub>peak</sub> value of PVC cable sheath compared to pure PVC could be attributed primarily to the formation of the volatile SbCl<sub>3</sub> due to the interaction of PVC and Sb<sub>2</sub>O<sub>3</sub> during thermal degradation [8]. Compared to pure PVC, four additional peaks can be observed for PVC cable sheath, two in the initial degradation stage, and two near the end of degradation.

Figure 2a presents the TG and DTG curves of PVC cable sheath in both air and nitrogen atmospheres at a heating rate of 10 K min<sup>-1</sup>. In addition to the two shoulder peaks, there are four mass loss peaks in the nitrogen atmosphere and five in the air atmosphere. The shoulder peaks, which appear before peak1, are due to degradation of plasticizers [6, 27]. The first peak (peak1) is mainly caused by the dehydrochlorination of PVC. In this process, the released HCl reacts with Sb<sub>3</sub>O<sub>2</sub> and forms the volatile SbCl<sub>3</sub>. This reaction absorbs heat and hence prevents the temperature of PVC from rising [28] and results in a decrease in the DTG<sub>peak</sub> value of peak1 compared to pure PVC [8] as shown in Fig. 1. Additionally,

**Fig. 1** TG results **a** DTG curves of pure PVC and PVC cable sheath in nitrogen **b** DTG curves of pure PVC and PVC cable sheath in air



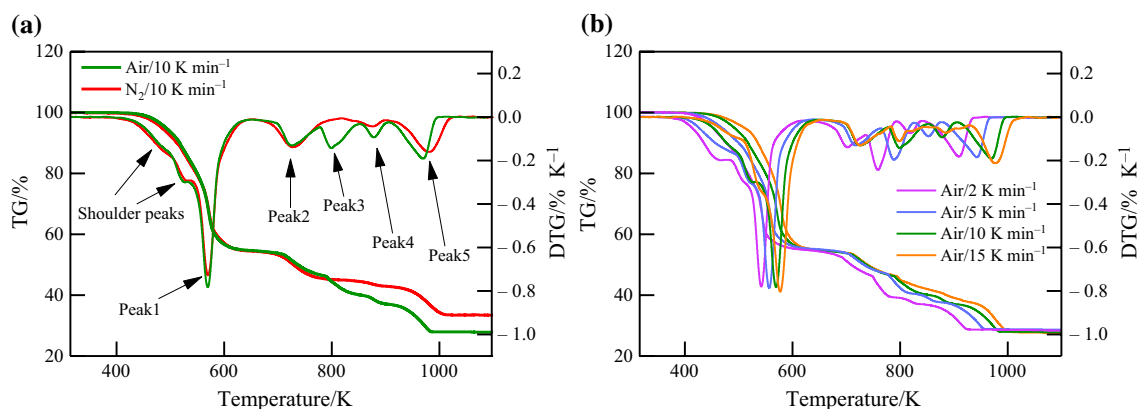


**Fig. 2** TG results **a** TG and DTG curves of PVC cable sheath in nitrogen and air at  $10 \text{ K min}^{-1}$ , **b** TG and DTG curves of PVC cable sheath in air at different heating rates

oxidative pyrolysis of PVC at low temperatures accelerates the formation process of HCl [29], which results in a larger value of peak1 in air. The second peak (peak2) is mainly due to the structural rearrangement of PVC and various additives [15]. A new peak (peak3) appears in the air atmosphere, which may be attributed to the combustion of carbon produced by the previous processes [14]. Due to the oxidation of additives such as flame retardant [8], the value of peak4 is higher in air. The last peak (peak5) in both nitrogen and air atmospheres is the slow decomposition of residues, including additives and fillers such as  $\text{CaCO}_3$  [5]. At the end of the test, the final residual mass under air and nitrogen is 27.8 and 33.3%, respectively.

Figure 2b presents a comparison of the TG and DTG results of PVC cable sheath under different heating rates. It can be observed that although, due to the heat transfer hysteresis, the DTG peaks are shifted to higher temperatures with an increase in the heating rate [6], the shape of TG/DTG curves and the final residual mass ( $27.8 \pm 0.1\%$ ) are effectively insensitive to the heating rate.

### FTIR analysis

The FTIR spectrum at different heating rates in air is similar, and the results at the heating rate of  $10 \text{ K min}^{-1}$  were selected as an example for analysis. Figure 3 shows the typical 3D FTIR spectrogram of the whole oxidative pyrolysis process.

It can be seen in Fig. 3 that a variety of gases are generated between 500 and 700 K and between 800 and 1000 K, while few in the range of 700–800 K, which is consistent with the distribution of peaks in Fig. 1a.

Figure 4 shows the FTIR spectra of PVC cable sheath at the temperatures corresponding to DTG peaks, and the characteristic absorption peaks of all gases produced by oxidative pyrolysis are listed in Table 1. For peak1, the

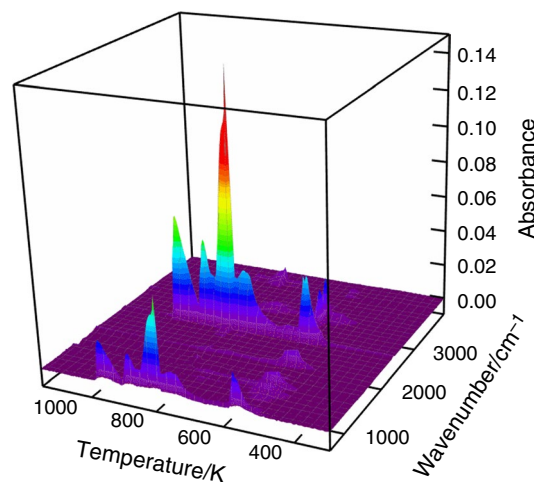


**Fig. 3** Typical FTIR 3D spectrogram

absorption spectrum band at  $3150\text{--}2600 \text{ cm}^{-1}$  is due to the H-Cl antisymmetric stretching vibration of HCl gas [30]. The absorption peak at  $2935 \text{ cm}^{-1}$  is indicative of the C-H stretching vibration of alkanes [31]. The absorption spectral bands at 669 and  $2359 \text{ cm}^{-1}$  correspond to the C=O in-plane/out-of-plane bending vibration [1] and C=O antisymmetric stretching vibration of  $\text{CO}_2$  [31], respectively. The C–O–C symmetric stretching vibration at  $1120 \text{ cm}^{-1}$ , C–O–C antisymmetric stretching vibration at  $1277 \text{ cm}^{-1}$ , and the C=O stretching vibration at  $1745 \text{ cm}^{-1}$  all belong to the ester group in the plasticizer [1]. The O–H symmetric stretching vibration and asymmetric stretching vibration at  $3500\text{--}3900 \text{ cm}^{-1}$  refer to  $\text{H}_2\text{O}$ . At peak3, the C–O stretching vibration at  $2000\text{--}2260 \text{ cm}^{-1}$  is assigned to CO [31].

Figures 5a and 5b depict the variation in gaseous products in the temperature ranges of 315–790 K and 750–1050 K, respectively. In Fig. 5a, the signal of the ester group due to the pyrolysis of plasticizer was detected in the same



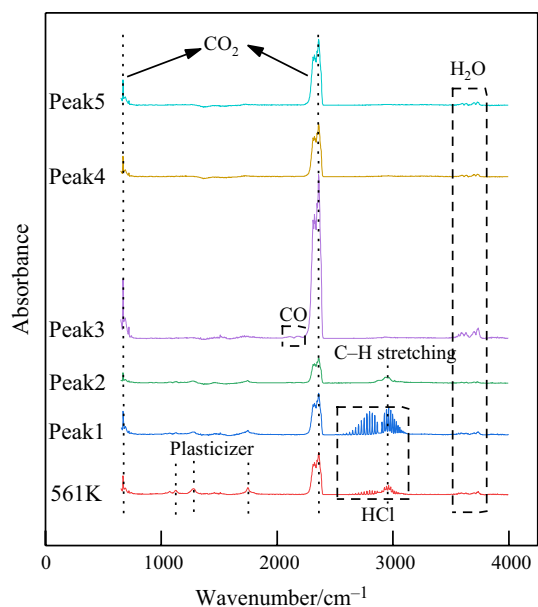


Fig. 4 FTIR spectra at different temperatures

temperature range as the DTG shoulder peaks. The release trend of HCl is well consistent with the peak1 in DTG curves. The curve of saturated hydrocarbon shows two peaks (peak1 and peak2). The production of CO<sub>2</sub> can be attributed to the decarboxylation of the ester groups [1] and the reaction between HCl and carbonate [5]. As can be seen in Fig. 5b, water, CO and CO<sub>2</sub> are released in the temperature range of 780–840 K, which is the result of combustion of char. For peak4 and peak5, the main gas product is CO<sub>2</sub> resulted from additives such as CaCO<sub>3</sub>.

Based on the above analysis, it can be summarized that the release of HCl, as well as the decomposition of the plasticizers and flame retardant, is mainly responsible for the shoulder peaks and peak1. The C-H stretching vibration corresponding to alkane appears during peak1 and peak2. H<sub>2</sub>O and CO<sub>2</sub> are generated continuously in the whole oxidative pyrolysis process. The maximum peak of CO appears near peak3.

### Deconvolution procedure and oxidative pyrolysis model

Figure 6 presents the differential DTG (DDTG) and deconvolution DTG curves of degradation of PVC cable sheath at

**Table 1** Summary of the vibration assignments

	Vibration	Peak position, cm <sup>-1</sup>
Hydrogen chloride	H-Cl asymmetric stretching	3150–2600
Saturated hydrocarbon	C-H stretching	2935
Plasticizer (ester group)	C–O–C symmetric stretching	1120
	C–O–C asymmetric stretching	1277
	C=O stretching	1745
	CO <sub>2</sub>	Out-of-plane/In-plane C=O bending
	C=O asymmetric stretching	2359
CO	C–O stretching	2179
H <sub>2</sub> O	O–H symmetric/asymmetric stretching	3736

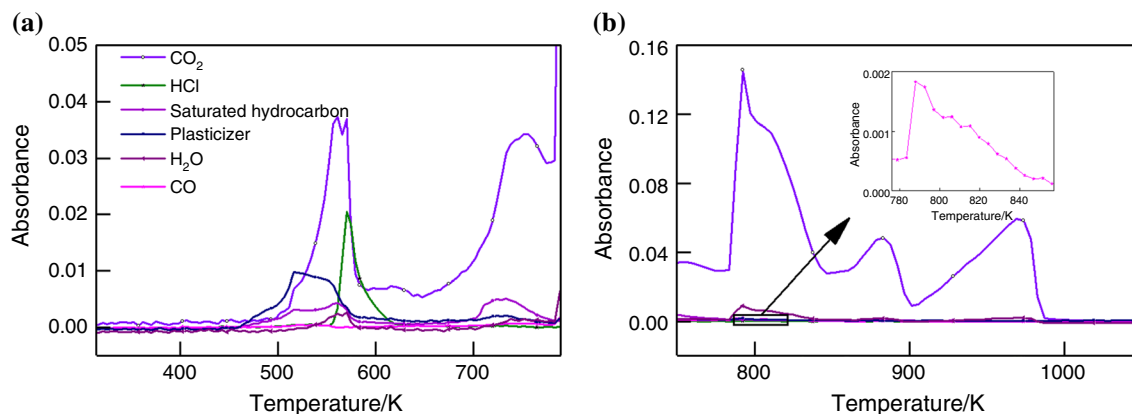
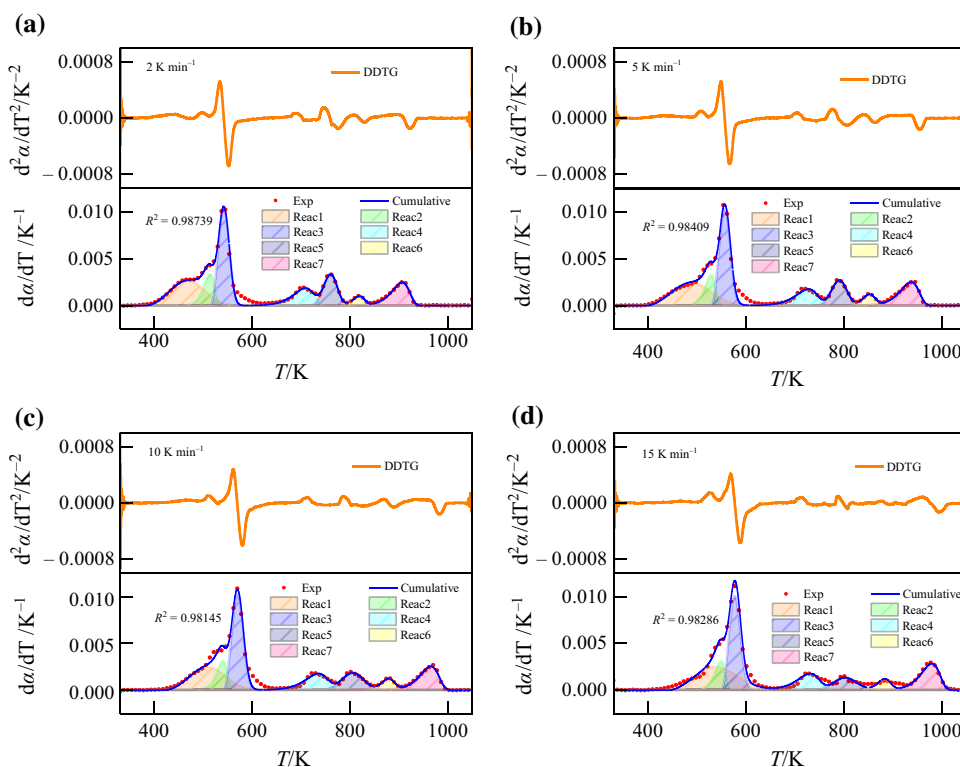


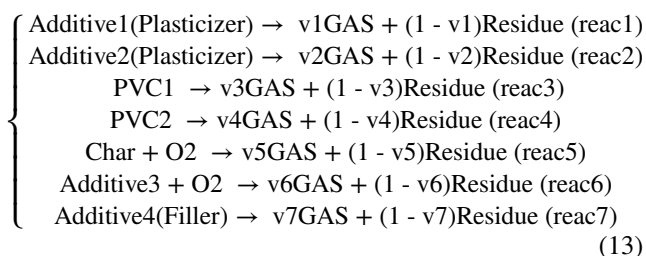
Fig. 5 History of evolved gaseous products as a function of temperature

**Fig. 6** DDTG and peak fitting curves for PVC cable sheath at different heating rates



different heating rates. In Fig. 6, at least seven local minimums can be distinguished in the DDTG curves. Considering the analysis in sections 3.1 and 3.2, the number of reaction steps was set as seven in the deconvolution procedure. Moreover, for each reaction step, the position of local minimums can provide an estimation of center values for the fitting function. By fitting the cumulative value of seven functions with the DTG data, the deconvolution procedure can be applied to determine all the constants ( $a_0$ ,  $a_1$ ,  $a_2$  and  $a_3$ ) in the functions (Table S2 in the Supplementary Materials). The correlation coefficient  $R^2$  is higher than 0.98 for all cases, which verifies the accuracy of the deconvolution results. Fitting errors mainly exist in the temperature range of 580–620 K, which might be caused by the complex reaction process of PVC dehydrochlorination [20] and the synergistic flame-retardancy effect between PVC and  $Sb_2O_3$  [32].

Parallel reaction is a common method to simulate the whole degradation process of PVC or cable materials [2, 7, 14]. Based on the results in Fig. 6 and previous analysis [2, 7, 14], a seven-step reaction model was proposed.



where Additive1, Additive2, Additive3, Additive4, PVC1, PVC2 and Char represent the pseudo-components in the parallel reactions and  $\nu$  denotes the mass fraction of evaporated gases for each reaction.

### Estimation of kinetic parameters

The activation energies calculated using the three model-free methods are shown in Fig. 7 as a function of the conversion degree  $\alpha$ , along with the maximum relative error for each reaction. The relative error is calculated as

$$\text{Relativeerror} = \left| \frac{E_{\text{method},\alpha} - \bar{E}}{\bar{E}} \right| \times 100\% \quad (14)$$

where  $\bar{E}$  is the mean value of activation energies obtained by the Friedman method,  $E_{\text{method},\alpha}$  denotes the activation energy at  $\alpha$  obtained by a certain method. It should be noted that all the activation energy discussed in the next sections is the mean value for each reaction unless otherwise stated.

For reactions 1–4, 6 and 7, the maximum relative errors are small (detail values shown in Fig. 7), which verifies the rationality and reliability of the 7-step reaction model. For the decomposition of plasticizers (reactions 1–2), its activation energy ( $54 \text{ kJ mol}^{-1}$ ,  $131 \text{ kJ mol}^{-1}$ ) is lower than that of the hydrochlorination reaction of PVC (reaction 3,  $144 \text{ kJ mol}^{-1}$ ). This can explain the phenomenon that the

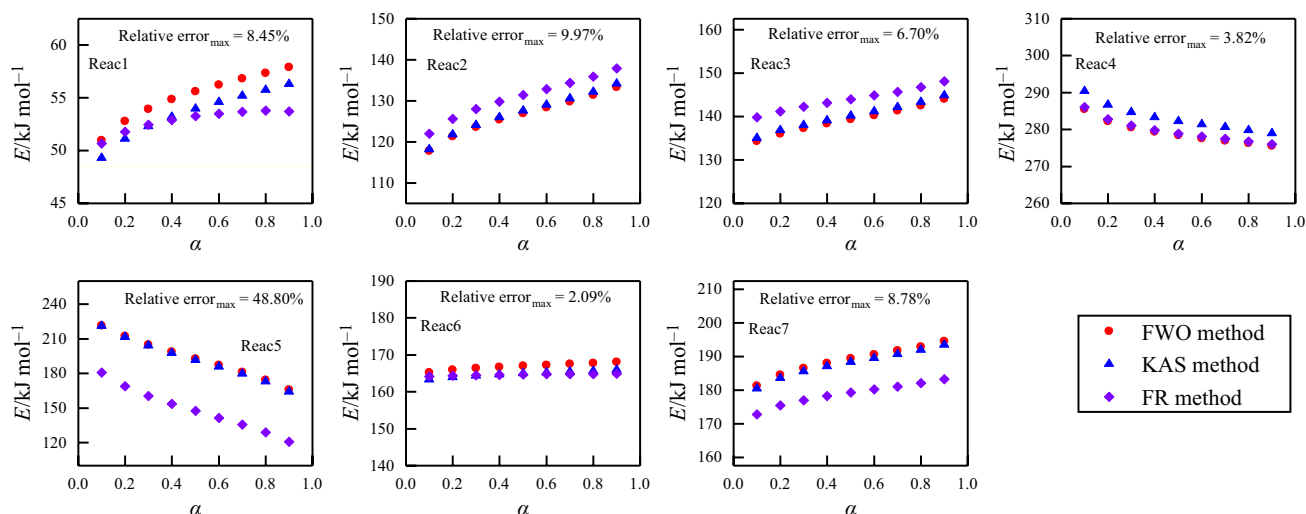
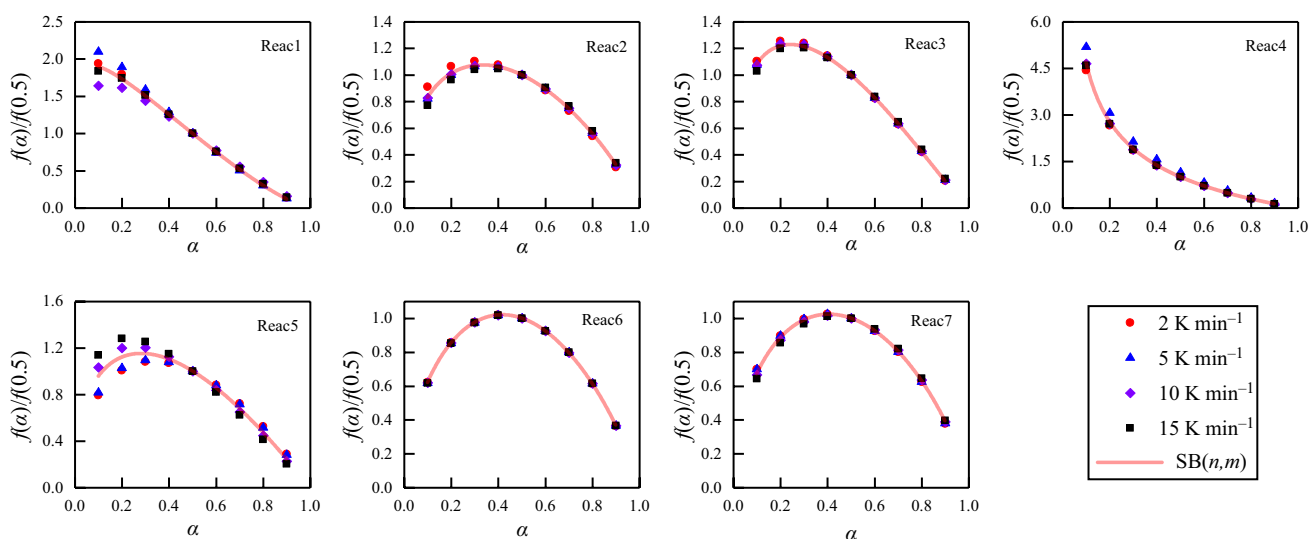


**Fig. 7** Activation energies obtained by model-free methods for each reaction

activation energy of PVC cable sheath increases with conversion degree at the initial pyrolysis stage of PVC [1]. The activation energy of the PVC decomposition process (reaction3 and reaction4) for PVC cable sheath is higher than that of pure PVC [33, 34], which can be attributed to the flame-retardant effect of  $\text{Sb}_2\text{O}_3$ . For reaction 5, the relative error is large with a maximum value of 48.8%, which could be attributed to the difference between differential isoconversional methods (FR) and integral isoconversional methods (KAS, FWO) [35].

By using Eq. (10), we can determine  $\frac{f(\alpha)}{f(0.5)}$  for different conversion degrees, and the results are shown in Fig. 8 for the four heating rates. The results show that  $\frac{f(\alpha)}{f(0.5)}$  is nearly

independent of the heating rate except for reactions 1 and 5 at low conversion degrees. Figure 8 also presents the non-linear curve fit using the Truncated Sestak-Berggren model (SB(m,n)) and the fitted parameters (AutocatPower m and Reaction order n) are shown in Table 2. The results indicate that the kinetic mechanisms of reactions 3 and 5 tilt toward autocatalytic models at low conversion degrees. By substituting the obtained values of  $E$  (FR method),  $f(\alpha)$  (Generalized master-plot method) into Eq. (10), the pre-exponential factor  $A$  can be calculated. The estimated kinetic triplets for each reaction are listed in Table 2.

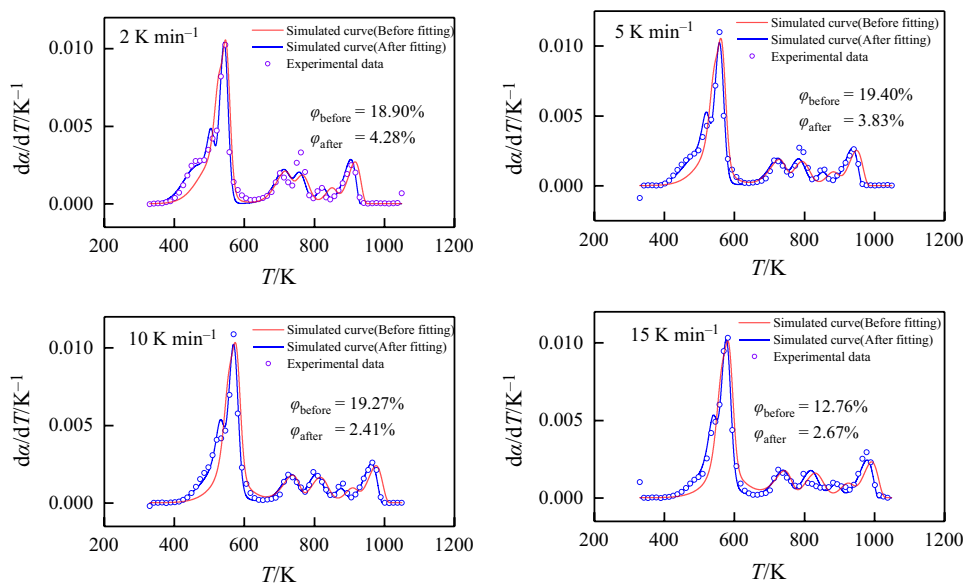


**Fig. 8** Fitted  $\text{SB}(n,m)$  models that well describe the independent reactions



**Table 2** Kinetic parameters (a) estimated for the oxidative pyrolysis model using the FR model and (b) optimized using the genetic algorithm (GA). The optimized data also include the reaction mechanism and associated model parameters for each reaction

		Reac1	Reac2	Reac3	Reac4	Reac5	Reac6	Reac7
Estimated	lnA (s <sup>-1</sup> )	10.06 ± 0.76	27.89 ± 1.80	29.33 ± 0.91	44.80 ± 0.84	21.11 ± 4.56	21.49 ± 0.05	22.15 ± 0.17
	E (kJ mol <sup>-1</sup> )	53.85 ± 3.54	130.86 ± 8.84	143.98 ± 4.17	279.67 ± 6.44	148.60 ± 32.06	164.62 ± 0.44	178.82 ± 6.05
	SB (n, m)	SB(1.36, 0.10)	SB(0.85, 0.43)	SB(1.13, 0.36)	SB(1.06, -0.58)	SB(1.03, 0.40)	SB(0.84, 0.61)	SB(0.77, 0.53)
Optimized	lnA (s <sup>-1</sup> )	10.04	28.78	30.10	45.06	22.48	23.44	22.18
	E (kJ mol <sup>-1</sup> )	49.50	127.05	143.13	280.14	154.98	173.32	182.85
	SB(n, m)	SB(1.35, 0.09)	SB(0.89, 0.41)	SB(1.12, 0.39)	SB(1.02, -0.56)	SB(0.98, 0.41)	SB(0.82, 0.59)	SB(0.70, 0.52)
	Fitted model	F1	A1.5	A1.5	D1	A1.5	A2	A2
	v (%)	22.22	8.15	32.63	10.23	10.45	3.70	12.62

**Fig. 9** Comparison of the simulated versus experimental data

### Parameter optimization and reaction mechanism

With the kinetic parameters determined in Table 2, we can construct the DTG curves and compare them with the experimental data as shown in Fig. 9. It can be seen that there are relatively large differences between the experimental and simulated values, with the fitting error  $\varphi$  reaching 19.40% for the test with the heating rate of 5 K min<sup>-1</sup>. To predict more accurately the thermal behavior of PVC cable materials, the estimated kinetic parameters in Table 2 were employed as the initial values for further optimization using the GA. The corresponding parameter ranges were set as  $\pm 10\%$  of the initial values. The whole optimizing process consisted of 35 parameters including  $A$ ,  $E$ ,  $n$ ,  $m$  and mass loss contribution  $v$  for each reaction. The predicted curves before and after optimization are shown in Fig. 9.

Figure 9 indicates that the fitting error  $\varphi$  is decreased substantially after the GA optimization. For example, the fitting

error of the 2 K min<sup>-1</sup> case decreases from 18.90 to 4.28%. The maximum fitting error occurs for reaction 5, in the temperature range of 750–850 K. This could be attributed to the carbon combustion reaction, in which the thermal behaviors were found to be dependent on the heating rate [36].

By comparing with the results obtained from the optimized SB(m,n) model in Fig. 10, we can also determine, for each of the reactions, the type of the reaction model (i.e., Power law model, Reaction order model, Nucleation growth mechanism model, and Diffusion model) and the associated model parameters. A comparison of the degradation process ( $\frac{f(\alpha)}{f(0.5)}$ ) as a function of  $\alpha$ ) obtained by the reaction model and the SB(m,n) model is presented in Fig. 10, which shows a good agreement between the two sets of data. The reaction models found are summarized in Table 2 along with the detailed model parameters: F1 for reaction 1; A1.5 for reactions 2, 3 and 5; D1 for reaction 4; and A2 for reactions 6 and 7.

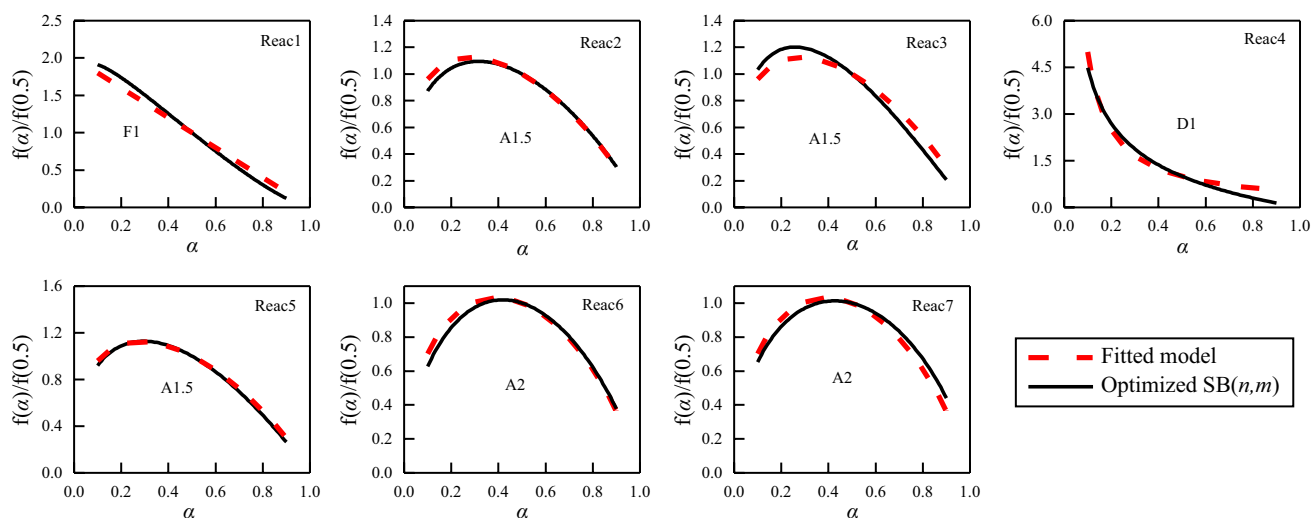


**Fig. 10** Reaction mechanism fitting result based on the optimized SB( $n, m$ ) model

## Conclusions

A series of TG-FTIR experiments was conducted at different heating rates to study the oxidative pyrolysis process of mining PVC cable sheath consisting of PVC resin, plasticizers (Phthalate esters), fillers (Calcium carbonate) and flame retardant (Antimony trioxide,  $\text{Sb}_2\text{O}_3$ ). The effects of the additives on the degradation and evolved gases of PVC were investigated and analyzed. The following conclusions can be obtained:

- (1) The oxidative pyrolysis of PVC cable sheath was more complex than that of pure PVC, which was manifested in the lower onset degradation temperature and the addition of two new mass loss peaks. The air atmosphere had a significant impact on the degradation of cable sheath materials, as demonstrated by an increased peak4 value (oxidation of flame retardants) and a new peak3 (combustion of carbon from previous reactions). The flame-retardant  $\text{Sb}_2\text{O}_3$  plays an important role in reducing the mass loss rate of PVC cable sheath as it reacts with the hydrochloric acid (HCl) released from PVC and forms the volatile  $\text{SbCl}_3$ , which absorbs heat and thence prevents the temperature of PVC from rising.
- (2) The dehydrochlorination of PVC, together with the decomposition of plasticizers, occurred near shoulder peaks and peak1. The C-H stretching vibration corresponding to saturated hydrocarbon appeared in peak1 and peak2.  $\text{H}_2\text{O}$  and  $\text{CO}_2$  were generated continuously during the whole mass loss process with their maximum peak values appearing at peak3, whereas CO was produced almost exclusively at peak3.

- (3) The whole decomposition process was divided into seven individual stages by using the deconvolution method and a corresponding seven-step oxidative pyrolysis model was proposed, including the pyrolysis of plasticizers, dehydrogenation, emission, and combustion of volatile fraction, carbon combustion, oxidative pyrolysis of additives, and the decomposition of fillers.
- (4) The kinetic triplets of each reaction were calculated and analyzed using three model-free methods and a generalized master-plots method. To accurately predict the thermal behavior of PVC cable sheath, the model parameters were further optimized using the genetic algorithm (GA) and it was found that the fitting error  $\varphi$  was decreased substantially after the optimization. Based on the optimized parameters, the reaction mechanism of each of the reactions and the associated model parameters were identified (Table 2).

**Supplementary Information** The online version contains supplementary material available at <https://doi.org/10.1007/s10973-022-11723-8>.

**Acknowledgements** This study was sponsored by the National Key R&D Program of China (2021YFB3201900), National Natural Science Foundation of China (No. 51906253 and No. 72091512), the Fundamental Research Funds for the Central Universities (No. 2021JCCXAQ01), Key Laboratory of Emergency Management Department of Fire Emergency Rescue Equipment (2019XFZB16)

**Author contributions** JZ contributed to conceptualization, investigation, methodology, writing—original draft. HM contributed to data curation, formal analysis, software. HH contributed to supervision, writing—review and editing. JZ contributed to methodology, supervision, writing—review and editing. YC contributed to writing—review and editing.

**Open Access** This article is licensed under a Creative Commons Attribution 4.0 International License, which permits use, sharing, adaptation, distribution and reproduction in any medium or format, as long as you give appropriate credit to the original author(s) and the source, provide a link to the Creative Commons licence, and indicate if changes were made. The images or other third party material in this article are included in the article's Creative Commons licence, unless indicated otherwise in a credit line to the material. If material is not included in the article's Creative Commons licence and your intended use is not permitted by statutory regulation or exceeds the permitted use, you will need to obtain permission directly from the copyright holder. To view a copy of this licence, visit <http://creativecommons.org/licenses/by/4.0/>.

## References

- Xue MY, Lu YH, Li K, et al. Thermal characterization and kinetic analysis of polyvinyl chloride containing Sn and Zn. *Therm Anal Calorim.* 2020;139:1479–92.
- Matala A, Hostikka S. Pyrolysis modelling of PVC cable materials. *Fire Saf Sci.* 2011;10:917–30.
- Zou Y, Li Y, Bourbigot S, et al. Determination of solid-phase reaction mechanism and chlorine migration behavior of co-pyrolyzing PVCCaCO<sub>3</sub> based polymer using temperature-dependent FTIR and XRD analysis. *Polym Degrad Stabil.* 2021;193:109741.
- Wang K, Jiang S, Ma X, et al. Information fusion of plume control and personnel escape during the emergency rescue of external-caused fire in a coal mine. *Process Saf Environ Prot.* 2016;103:46–59.
- Beneš M, Milanov N, Matuschek G, et al. Thermal degradation of PVC cable insulation studied by simultaneous TG-FTIR and TG-EGA methods. *J Therm Anal Calorim.* 2004;78(2):621–30.
- Brebu M, Vasile C, Antonie SR, et al. Study of the natural ageing of PVC insulation for electrical cables. *Polym Degrad Stabil.* 2000;67(2):209–21.
- Tang X, Xie Q, Qiu R, et al. Development of a relationship between kinetic triplets and heating rates to improve pyrolysis kinetic modeling of polymer. *Polym Degrad Stabil.* 2018;154:10–26.
- Wang Z, Wei R, Wang X, et al. Pyrolysis and combustion of polyvinyl chloride (PVC) sheath for new and aged cables via thermogravimetric analysis-Fourier transform infrared (TG-FTIR) and calorimeter. *Materials.* 2018;11(10):1997.
- Wang Z, Wang J. A comprehensive study on the flame propagation of the horizontal laboratory wires and flame-retardant cables at different thermal circumstances. *Process Saf Environ Prot.* 2020;139:325–33.
- Wang C, Liu H, Zhang J, et al. Thermal degradation of flame-retarded high-voltage cable sheath and insulation via TG-FTIR. *J Anal Appl Pyrolysis.* 2018;134:167–75.
- Zhou J, Liu G, Wang S, et al. TG-FTIR and Py-GC/MS study of the pyrolysis mechanism and composition of volatiles from flash pyrolysis of PVC. *J Energy Inst.* 2020;93(6):2362–70.
- Aracil I, Font R, Conesa JA. Thermo-oxidative decomposition of polyvinyl chloride. *J Anal Appl Pyrolysis.* 2005;74(1–2):215–23.
- Bhargava A, Van Hees P, Andersson B. Pyrolysis modeling of PVC and PMMA using a distributed reactivity model. *Polym Degrad Stabil.* 2016;129:199–211.
- Wang Q, Wang G, Zhang J, et al. Combustion behaviors and kinetics analysis of coal, biomass and plastic. *Thermochim Acta.* 2018;669:140–8.
- Wang Z, Xie T, Ning X, et al. Thermal degradation kinetics study of polyvinyl chloride (PVC) sheath for new and aged cables. *Waste Manage.* 2019;99:146–53.
- Vyazovkin S, Burnham AK, Criado JM, et al. ICTAC Kinetics Committee recommendations for performing kinetic computations on thermal analysis data. *Thermochim Acta.* 2011;520(1–2):1–19.
- Vyazovkin S, Burnham AK, Favregeon L, et al. ICTAC Kinetics Committee recommendations for analysis of multi-step kinetics. *Thermochim Acta.* 2020;689:178597.
- Cai J, Alimujiang S. Kinetic analysis of wheat straw oxidative pyrolysis using thermogravimetric analysis: statistical description and isoconversional kinetic analysis. *Ind Eng Chem Res.* 2009;48(2):619–24.
- Janković B, Adnadević B, Kolar-Anić L, et al. The non-isothermal thermogravimetric tests of animal bones combustion. Part II. Statistical analysis: Application of the Weibull mixture model. *Thermochim Acta.* 2010;505(1–2):98–105.
- Perejón A, Sánchez-Jiménez PE, Criado JM, et al. Kinetic analysis of complex solid-state reactions: A new deconvolution procedure. *J Phys Chem B.* 2011;115(8):1780–91.
- Doyle CD. Estimating isothermal life from thermogravimetric data. *J Appl Polym Sci.* 1962;6:639–42.
- Ozawa T. A new method of analyzing thermogravimetric data. *Bull Chem Soc Jpn.* 1965;38(11):1881–6.
- Flynn JH, Wall LA. A quick, direct method for the determination of activation energy from thermogravimetric data. *J Polym Sci Part B Polym Lett.* 1966;4(5):323–8.
- Kissinger HE. Variation of peak temperature with heating rate in differential thermal analysis. *Res Natl Bur Stand.* 1956;57(4):217–21.
- Friedman HL. Kinetics of thermal degradation of char-forming plastics from thermogravimetry. Application to a phenolic plastic. *J Polym Sci Part C Polym Symp.* 1964;6(1):183–95.
- Sánchez-Jiménez PE, Pérez-Maqueda LA, Perejón A, et al. Generalized master plots as a straightforward approach for determining the kinetic model: the case of cellulose pyrolysis. *Thermochim Acta.* 2013;552:54–9.
- Wang YH, Wu WH, Meng WH, et al. Activated carbon spheres@NiCo<sub>2</sub>(CO<sub>3</sub>)<sub>1.5</sub>(OH)<sub>3</sub> hybrid material modified by ionic liquids and its effects on flame retardant and mechanical properties of PVC. *Composites Part B.* 2019;179:107543.
- Yoshinaga S, Matsumoto M, Nagaishi T, et al. The pyrolysis of poly(vinyl chloride) containing antimony(III) Oxide. *Nippon Kagaku Kaishi.* 1973;1:175–82.
- Wang L, Zhang R, Deng R, et al. Oxygen-induced enhancement in low-temperature dechlorination of PVC: An experimental and DFT study on the oxidative pyrolysis process. *ACS Sustainable Chem Eng.* 2021;9(7):2835–43.
- Wu J, Chen T, Luo X, et al. TG/FTIR analysis on co-pyrolysis behavior of PE, PVC and PS. *Waste Manage.* 2014;34(3):676–82.
- Gao N, Li A, Quan C, et al. TG-FTIR and Py-GC/MS analysis on pyrolysis and combustion of pine sawdust. *J Anal Appl Pyrolysis.* 2013;100:26–32.
- Lum RM. Antimony oxide-PVC synergism: Laser pyrolysis studies of the interaction mechanism. *J Polym Sci Polym Chem Ed.* 1977;15(2):489–97.
- Sánchez-Jiménez PE, Perejón A, Criado JM, et al. Kinetic model for thermal dehydrochlorination of poly(vinyl chloride). *Polymer.* 2010;51:3998–4007.
- Slapak MJP, Van Kasteren JMN, Drinkenburg AAH. Determination of the pyrolytic degradation kinetics of virgin-PVC and PVC-waste by analytical and computational methods. *Comput Theor Polym Sci.* 2000;10(6):481–9.
- Janković B, Manić N. Kinetic analysis and reaction mechanism of p-alkoxybenzyl alcohol ([4-(hydroxymethyl) phenoxyethyl])

- polystyrene) resin pyrolysis: Revealing new information on thermal stability. *Polym Degrad Stabil.* 2021;189:109606.
36. Liu X, Tan H, Wang X, et al. Oxidation reactivity and kinetic analysis of bituminous coal char from high-temperature pyrolysis: Effect of heating rate and pyrolysis temperature. *Thermochim Acta.* 2020;690:178660.

**Publisher's Note** Springer Nature remains neutral with regard to jurisdictional claims in published maps and institutional affiliations.